COASTING p-p COLLIDING BEAM MACHINES

E Keil & N Marshall King

SUMMARY

The designs considered cover the energy range 20 TeV to 100 TeV per proton beam, with collisions taking place at small crossing angle. The crossing angle and luminosity are optimized at each energy. With single-turn filling of the storage rings, luminosities per intersection of order 10^{32} cm^{-2} sec^{-1} can be achieved throughout most of the energy range, provided that the incoming momentum spread from the injector synchrotron is blown up for storage. The ring lattices follow closely on design principles for lower energy machines, but invoke the use of 10 T superconducting dipoles and correspondingly high-gradient quadrupoles.

1. NORMAL CELL LATTICE

To arrive at design parameters for the normal cell lattices, the following strategy is adopted:

i) Fields and Gradients

Assuming niobium-tin superconductor to be a well-established choice by the time these large machines would be constructed, the dipole field is taken to be B = 10 T throughout. We envisage that this value of field will correspond to a few centimetres coil radius in a practical magnet design. The resulting bending radius, ρ, and total length of dipole in the ring, $(\ell_B)_{tot}$, are then given by:

$$\rho = \frac{10}{c_o} \cdot \frac{P}{B} = \frac{P}{c_o} \quad , \qquad \text{.....(1)}$$

$$(\ell_B)_{tot} = 2\pi\rho \quad , \qquad \text{.....(1a)}$$

for ρ and $(\ell_B)_{tot}$ in km, P in TeV/c, B in Tesla, and where $c_o = 2.997925 = c/10^8$ m/s.

To quote a maximum quadrupole gradient k_{max}, the difficulty is that some practical inner coil radius r_Q has to be estimated at which some field B_Q may be achieved, where $B_Q < 10$ T. Provisionally, we take:

$$k \lesssim k_{max} = 250 \text{ T/m} , \qquad .....(2)$$

corresponding to, say,

$$B_Q = 6.25 \text{ T at } r_Q = 2.5 \text{ cm} . \qquad .....(2a)$$

However, since we lack practical magnet design information for niobium-tin superconducting quadrupoles at present, we shall consider a wide range of k values.

The usual lattice gradient parameter K is given by:

$$K = c_o \times 10^{-4} \, k/P , \qquad .....(2b)$$

where K is in m^{-2}, k in T/m and P in TeV/c.

ii) Phase Advance, Lattice Functions

Choosing a simple FODO cell structure, as sketched in Fig 1, we take $\pi/2$ phase advance per cell. A thin lens analysis, with $K_F = K_D$, then leads to the approximate relations:

$$\mu_{np} \simeq \pi/2 , \quad Q_{np} \simeq N_p/4 , \qquad .....(3)$$

$$\ell_Q \ell_p \simeq 2\sqrt{2}/K , \qquad .....(3a)$$

$$\beta_{F,D} \simeq (1 \pm \tfrac{1}{2}\sqrt{2}) . \ell_p , \qquad .....(3b)$$

$$\eta_{F,D} \simeq \tfrac{1}{2}(1 \pm 0.25\sqrt{2}) \, \ell_p \theta , \; \theta = 2\pi/N_p . \qquad .....(3c)$$

Here, the subscript 'np' refers to normal periods: contributions from the insertions are neglected for the moment. The number of normal cells is N_p, their length is ℓ_p, and the length of each quadrupole is ℓ_Q.

iii) Geometry of Normal Cells

Following lower-energy lattice designs, the ratio of mean radius to bending radius in the normal cell part of the ring is taken to be 1.6 :

$$R_{np}/\rho = 1.6 = \ell_p/\ell_B \ , \quad \text{giving : } \ell_B = 0.625\ \ell_p \ . \qquad .....(4)$$

Similarly, the ratio of space in a period occupied by quadrupoles to the space left unoccupied by dipoles is taken to be 0.6 :

$$2\ell_Q/(\ell_p - \ell_B) = 0.6 \ , \text{ giving : } \quad \ell_Q = 0.1125\ \ell_p \ . \qquad .....(4a)$$

The remaining free space for correction elements, diagnostic equipment, bellows, flanges, etc, is given by:

$$\ell_s = 0.15\ \ell_p \ . \qquad .....(4b)$$

Combining the thin lens result (3a) with equs. (4a) and (2b), a lower limit for the period length ℓ_p is obtained :

$$\ell_p \geq (2.8959/k_{max}^{\frac{1}{2}}).\ P^{\frac{1}{2}} = c_1.\ P^{\frac{1}{2}} \ , \qquad .....(5)$$

where ℓ_p is in m, P in TeV/c, and k_{max} in T/m. For the equ.(2) value of k_{max}, 250 T/m, this corresponds to :

$$\ell_p \geq 18.3154\ .\ P^{\frac{1}{2}} \ . \qquad .....(5a)$$

Using equs.(1), (4) and (5), the corresponding upper limit for the number of normal cells is given by :

$$N_p \leq (3.2\pi \times 10^3/c_o\ c_1)\ .\ P^{\frac{1}{2}} \ , \qquad .....(5b)$$

$$= 183.1 \times P^{\frac{1}{2}} \ , \text{ for } k_{max} = 250 \text{ T/m} \ . \qquad .....(5c)$$

iv) Superperiod Considerations

Assuming that these large machines should have at least 8 interaction regions, we choose superperiodicity S = 8, and take N_p to be the largest integer divisible by 8, consistent with equ.(5c). The resulting normal cell lattice parameters are given in Table I, where the bracketed values are the result of subsequent accurate matching in the 'AGS' computer program.

TABLE I

NORMAL CELL LATTICE PARAMETERS

P(TeV/c)	20	40	60	80	100
ρ(km)	6.671	13.34	20.01	26.685	33.35
C_{np}(km)	67.06	134.1	201.2	268.3	335.3
N_p	816	1152	1408	1632	1824
ℓ_p(m)	82.19	116.4	142.9	164.4	183.85
$\frac{1}{2}\ell_B$(m)	25.68	36.39	44.66	51.37	57.45
$\frac{1}{2}\theta$(mrad)	3.85	2.73	2.23	1.925	1.72
ℓ_Q(m)	9.25 (10.0)	13.10 (14.15)	16.08 (17.36)	18.49 (20.0)	20.68 (22.34)
K(m^{-2})	3.75×10^{-3} (3.77×10^{-3})	1.87×10^{-3} (1.88×10^{-3})	1.25×10^{-3} (1.25×10^{-3})	0.937×10^{-3} (0.941×10^{-3})	0.750×10^{-3} (0.753×10^{-3})
$\frac{1}{4}\ell_s$(m)	3.08 (2.71)	4.37 (3.84)	5.36 (4.72)	6.16 (5.41)	6.89 (6.07)
Q_{np}	204.25	288.25	352.25	408.25	456.25
β_F(m)	136.2	193.0	236.9	272.4	304.7
β_D(m)	24.7	35.0	43.0	49.4	55.3
η_F(m)	0.424	0.426	0.428	0.425	0.425
γ_T	189.1	266.8	326.1	377.9	422.4

The chief result of the accurate matching calculation, compared with the thin lens approximation, is that the quadrupole lengths ℓ_Q have had to be augmented at the expense of ℓ_s. Accordingly, equs.(4a) and (4b) should be replaced by:

$$2\ell_Q/(\ell_p - \ell_B) = 0.648 \; ; \; \ell_Q = 0.1215\ell_p \; ; \; \ell_s = 0.132 \; \ell_p \; . \qquad .....(6)$$

These are the values used when calculating the luminosity and associated parameters at the crossing points.

2. INJECTION CONSIDERATIONS

We envisage injection from a chain of synchrotrons, the final one having much the same lattice geometry as the storage rings, - in particular, having the same 10 T peak field. Its minimum field should be in the region of 0.25 T if non-linear field effects in the superconducting dipoles at injection are to be kept to a safe level: hence, the final synchrotron would accelerate over a factor of about 40 in energy. Consequently, the penultimate synchrotron of the chain for the 20 TeV case would be a machine of about 0.5 TeV.

This brings us on to familar ground, and we may assume that such a machine has properties not unlike the existing CERN SPS and FNAL synchrotrons.

For instance, its mean radius could be about 1 km, (or less if it uses super-conducting magnets), so that about 10 of its pulses could be used to fill one turn of the 20 TeV synchrotron, in box car fashion. Allowing for some future improvements in circulating flux and in fast ejection technique, we envisage 6×10^{13} ejected protons per pulse, so that the number of protons in the 20 TeV ring for single-turn filling would be:

$$N \simeq 6 \times 10^{14} \qquad .....(7)$$

Since, at these high energies, stored energy in the beam begins to loom large as a problem in emergency conditions - eg. 1.92 GJ at 20 TeV - we shall assume that no further stacking is contemplated in the storage ring. We shall retain this value of the total number of protons in all the designs from 20 TeV to 100 TeV, so that the consequent line density decreases linearly with energy.

Next, the presence of an SPS-type synchrotron in the chain allows us to propose a value for invarient normalized transverse emittances, ε_t. We assume that ε_t does not become diluted significantly during subsequent transfers from one ring to another, and persists at the following value all the way through to the storage ring:

$$\varepsilon_t \approx 30\pi \times 10^{-6} \text{ m x rad} . \qquad .....(8)$$

In the storage ring, this emittance may be defined in terms of the rms beam radius σ^* and the betatron function β^*, at the crossing point:

$$\varepsilon_t = 4\pi.(\beta\gamma).\sigma^{*2}/\beta^* . \qquad .....(8a)$$

This last relation will be used later to evaluate the rôle of σ^* in the scaling of interaction point parameters with energy.

Finally, a similar identification of an SPS-type machine with one of the injector synchrotrons serves to define a normalized longitudinal emittance. Scaling to the 20 TeV machine, the SPS momentum spread of about 2×10^{-3} corresponds to a debunched $\Delta(\beta\gamma)$ value given by:

$$\Delta(\beta\gamma)_{20 \text{ TeV}} = 1.3 \times 10^{-2} . \qquad .....(9)$$

This provides a scale for normalized longitudinal emittance ε_ℓ in the coasting beam of the storage ring:

$$\varepsilon_\ell = \Delta(\beta\gamma).\ 2\pi R \ , \qquad .....(9a)$$

where R is the mean radius of the complete machine, including the insertions. Allotting 12 km to the insertion regions in the 20 TeV machine:

$$\varepsilon_\ell \approx 1.0 \times 10^3 \text{ m} \qquad .....(9b)$$

is the invariant value of longitudinal emittance.

On the assumption that the beam is not allowed to debunch in the chain of synchrotrons, the injection parameter $\Delta(\beta\gamma)_{inj} = \beta\gamma.\Delta P/P$ corresponding to a bunched beam, is allowed to vary as $P^{\frac{1}{2}}$ for the higher energy storage rings. As will be remarked in Section 5, this assumption does not affect our argument, since the debunched value $\Delta(\beta\gamma)_{st}$ required for coasting beam storage turns out to be much larger.

3. LUMINOSITY, ASSOCIATED PARAMETERS, AND SCALING LAWS

A procedure for determining optimum luminosity, crossing angle and β-value at the crossing point in coasting beam p-p storage rings has been described by one of the present authors.[1] The significant formulae are:-

$$L \simeq \frac{4}{3}\gamma \left[\frac{\pi \cdot \Delta\nu \cdot I^3}{e^3 c r_p \varepsilon_t . \ell_{int}} \right]^{\frac{1}{2}} , \qquad \ldots (10)$$

$$\beta^* \simeq \left[\frac{ec \cdot \Delta\nu . \varepsilon_t . \ell_{int}}{8\pi r_p I} \right]^{\frac{1}{2}} , \qquad \ldots (11)$$

$$\alpha \simeq \left(\frac{2}{\pi}\right)^{\frac{1}{2}} \frac{r_p I \beta^*}{ec . \Delta\nu . \gamma\sigma^*} . \qquad \ldots (12)$$

In these expressions, the notation is:

L = Luminosity per intersection, $(m^{-2}s^{-1})$,

$\Delta\nu$ = Limiting beam-beam tune shift, taken to be 0.005.

I = Proton current, (amp) = $Nec/2\pi R$, with $N = 6 \times 10^{14}$, (equ. 7).

r_p = Classical proton radius = 1.5347×10^{-18}m.

ε_t = Normalized transverse emittance = $4\pi(\beta\gamma)\sigma^{*2}/\beta^*$, (equ. 8a).
= $30\pi \times 10^{-6}$m, (equ. 8),

ℓ_{int} = Free space each side of the crossing point, (m). (cf. Fig 2).

β^* = Value of betatron function at the crossing point, (m).

α = Crossing angle, (rad).

σ^* = RMS beam radius at crossing point, (m), (equs. 8 and 8a).

γ = E/Eo; $c=2.997925 \times 10^8$ ms^{-1}; $e = 1.602 \times 10^{-19}$ coul.

In considering how the interaction point parameters scale with energy, the length ℓ_{int} plays an important part. Leaving its rôle unspecified for the moment, equs. (8a), (10), (11), and (12) show that:-

$$L \sim (\gamma \ell_{int})^{-\frac{1}{2}}$$

$$\beta^* \sim (\gamma \ell_{int})^{\frac{1}{2}}$$

$$\sigma^* \sim (\ell_{int}/\gamma)^{\frac{1}{4}} \qquad \ldots (13)$$
$$\alpha \sim (\ell_{int}/\gamma^5)^{\frac{1}{4}} ,$$

since ε_t, $\Delta\nu$ are constant, and since $I \sim \gamma^{-1}$ for constant N.

Referring to Fig 2, $(\alpha\ell_{int})$ is seen to determine the separation of beam centres, d_1, at the first magnetic element they encounter each side of the interaction point. Equs. (10)-(12) are valid only when the beams are sufficiently well-separated: we shall express d_1 in terms of some multiple 'm' of the local rms beam radius σ, and shall later interpret m=4 to mean 'sufficient separation':

$$d_1 \simeq \alpha\ell_{int} \sim (\ell_{int}/\gamma)^{5/4} , \qquad \ldots (14)$$
$$\alpha\ell_{int} \geq m\,\sigma , \qquad \ldots (14a)$$
$$\sigma^2 = \sigma^{*2} + (\varepsilon_t \ell_{int}/4\pi\gamma\sigma^*)^2 . \qquad \ldots (14b)$$

Using equs. (12),(11), (14b) and (8a) in equ. (14a), a lower limit is obtained for ℓ_{int}:

$$\ell_{int} \geq \frac{m^2 C.\Delta\nu.\varepsilon_t}{8Nr_p} \left[1 + \{\, 1 + \frac{2}{m^2\pi} \,\}^{\frac{1}{2}}\right] ,$$

or, ignoring the last small factor on the right hand side,

$$\ell_{int} \geq \frac{m^2 C.\Delta\nu.\varepsilon_t}{4Nr_p} \sim \gamma, \qquad \ldots (15)$$

where $C = 2\pi R$ is the total circumference of the ring.

With m = 4 at 20 TeV, allowing a total 12 km for the 8 insertions, the resulting minimum value for ℓ_{int} would be 162 m. We shall use the scale:

$$\ell_{int} = 8.75P, \qquad \ldots (15a)$$

where ℓ_{int} is in m for P in TeV/c.

Returning to equ. (13), the scaling laws are now seen to be:

$$\left.\begin{aligned} L &\sim \gamma^{-1}\ , \\ \beta^* &\sim \gamma\ , \\ \sigma^* &\sim \gamma^{o}\ , \\ \alpha &\sim \gamma^{-1}\ . \end{aligned}\right\} \qquad \ldots (16)$$

Recalling that the proton current I is defined by Nec/C, all the significant parameters at the crossing point may now be computed once the total circumference C has been defined. This requires further examination of the insertions.

4. THE INSERTIONS

Fig 2 illustrates schematically our present notion of a half-insertion. At the end of the free space ℓ_{int}, a dipole of length ℓ_1 and field B_1 diverts the opposing beams : after a further distance ℓ_2, they are separated by an amount $2d_2$, sufficient for locating the first sets of quadrupoles. Neglecting the small initial separation d_1 occasioned by crossing angle, d_2 is given by:

$$d_2 = c_o \times 10^{-4}.\ \ell_1\ell_2B_1/P \ \gtrsim 0.5\text{m, say.} \qquad \ldots (17)$$

Taking B_1 = 10T and ℓ_1 = 20m, then at P = 20 TeV/c this condition is met by $\ell_2 \gtrsim 167$m. We shall adopt these values for B_1 and ℓ_1 throughout; and, since the minimum value of ℓ_2 is close to ℓ_{int}, we shall equate these two lengths:

$$\left.\begin{aligned} B_1 &= 10\text{T} \\ \ell_1 &= 20\text{m} \\ \ell_2 &= \ell_{int} = 8.75P,\ (\text{m, TeV/c}) \\ d_2 &= 0.525\text{m} \end{aligned}\right\} \qquad \ldots (17a)$$

It may prove possible to reduce ℓ_2 in a more detailed design, (eg. using greater values of ℓ_1 at the higher energies), but at present we take the view that allowing ℓ_2 to vary as γ will permit easier matching conditions for the high-β quadrupoles, and will also be consistent with the experimental physics requirements.

Similarly, considering the remainder of the insertion - length ℓ_3 in Fig 2 - rough scaling arguments based on insertion matching and on chromaticity correction lead us to propose, as a conservative choice:

$$\ell_3 \simeq (\ell_{int} + \ell_2) \sim \gamma. \qquad \ldots (17b)$$

Detailed consideration may allow this length to be reduced in a final design. However, using equ (17b), the length of a half-insertion is given by $4\,\ell_{int}$, and we define:

$$\ell_{ins} = 8\,\ell_{int} = 70P, \text{ (m, TeV/c)}, \qquad \ldots (18)$$

$$(\ell_{ins})_{tot} = 8\,\ell_{ins} = 0.560P, \text{ (km, TeV/c)}, \qquad \ldots (18a)$$

$$C = C_{np} + (\ell_{ins})_{tot} = (3.3534+0.560).\ P = 3.913.P, \text{(km, TeV/c)}.. \qquad (18b)$$

With constant proton flux of 6×10^{14}, the coasting beam current is then given by:

$$I = Nec/C = 7.364.P^{-1}, \text{ (amp, TeV/c)}, \qquad \ldots (19)$$

and the proton line density λ by:

$$\lambda = N/C = 1.533 \times 10^{14}.\ P^{-1}, \text{ (km}^{-1}\text{, TeV/c)}. \qquad \ldots (19a)$$

The stored energy in the beam is:

$$W = NeE \simeq 0.0961.P, \text{ (GJ, TeV/c)}. \qquad \ldots (20)$$

Each insertion will contribute a phase shift π to the total machine tune, so that:

$$Q = Q_{np} + 4. \qquad \ldots (21)$$

5. CALCULATED STORAGE RING PARAMETERS

The equations quoted in Sections 2,3 and 4 allow most of the important storage ring parameters to be calculated, and Table I may now be complemented by the quantities listed in Table II. The interaction point parameters L,β*, α and ℓ_{int} are also plotted in Figs. 3-6.

TABLE II

STORAGE RING PARAMETERS

ADDITIONAL TO TABLE I

P (TeV/c)	20	40	60	80	100
C (km)	78.26	156.5	234.8	313.0	391.3
R (km)	12.46	24.91	37.37	49.82	62.28
ℓ_{int} (km)	0.175	0.350	0.525	0.700	0.875
ℓ_{ins} (km)	1.4	2.8	4.2	5.6	7.0
I (amp)	0.364	0.182	0.121	0.091	0.073
W (GJ)	1.92	3.84	5.76	7.68	9.60
Q	208.25	292.25	356.25	412.25	460.25
L ($cm^{-2}s^{-1}$)	4.06×10^{32}	2.03×10^{32}	1.35×10^{32}	1.02×10^{32}	0.813×10^{32}
β^* (m)	16.79	33.57	50.38	67.16	83.92
σ^* (μm)	79.32	79.29	79.34	79.32	79.29
α (μrad)	30.95	15.48	10.31	7.737	6.191
$\Delta(\beta\gamma)_{inj}$	0.013	0.0184	0.0225	0.0260	0.0291
$\Delta(\beta\gamma)_{st}$	4.00	6.73	9.12	11.32	13.38

These results have been checked using the CERN program STORPA2. Besides calculating the above parameters, this code incorporates all the single beam limiting phenomena discussed in Ref. (1) - incoherent tune shift, transverse and longitudinal resistive wall instabilities, as well as the "stored energy limited current" defined by:

$$I_w = WB/2\pi \ (m_p c/e)^2 \ (R/\rho)\gamma^2 \qquad \ldots (22)$$

In accord with the Ref. (1) discussion, the following parameters were specified to cover these additional features:

$$\begin{array}{ll} \text{Incoherent tune shift limit,} & \Delta Q \lesssim 0.025 \\ \text{Transverse resistive wall tune spread} & \delta Q \gtrsim 0.02 \\ \text{Resistive wall mode number,} & (n-Q)=0.75 \\ \text{Conductivity of vacuum chamber wall,} & \sigma_c = 10^6 \text{ A/Vm} \end{array} \qquad \ldots (23)$$

Further, the computations covered a range of different aperture radii 'b' for different values of maximum quadrupole field B_Q at the inner coil radius:

$$2\text{cm} \lesssim b \lesssim 6\text{cm} \ , \ 4\text{T} \lesssim B_Q \lesssim 10\text{T} \qquad \ldots (24)$$

In no case did any of the single beam limits affect the argument: the corresponding limiting currents were always greater than those quoted in Table II: the luminosity and crossing point parameters of Table II were always attainable for single-turn filling of 6×10^{14} protons into the storage rings.

One significant outcome of this wide survey concerned the momentum spread required in the stored beam. As seen in the last row of Table II (for k = 250T/m) the $\Delta(\beta\gamma)_{st}$ spread is many times that present in the injected beam from the synchrotron, (cf. penultimate row of Table II). This effect is very dependent upon the parameters of the normal cell part of the lattice. Figs 7 and 8 show how the Q_{np} and $\Delta(\beta\gamma)_{st}$ vary for different values of k_{max}, (corresponding to any relevant choice of 'b' and B_Q within the equ (24) range). The factor of blow-up required is reduced for lower Q-values, as suggested by the η-variation of equ (3c).

This effect places demands on the RF system, examined briefly in the next Section.

6. RF VOLTAGES REQUIRED

The RF voltage required for stationary buckets of half height $\Delta(\beta\gamma)$ is given by:

$$V_{RF} = \left[\frac{\Delta(\beta\gamma)}{Q}\right]^2 . \frac{R}{\gamma} . (\pi^2 . f_{RF} . m_p c/e). \qquad \ldots (25)$$

Choosing f_{RF} = 200 MHz, as in the SPS, this formula reduces to:

$$V_{RF} = 6.178 \times 10^6 . \frac{R}{\gamma} . \left[\frac{\Delta(\beta\gamma)}{Q}\right]^2 \qquad \ldots (25a)$$

where V_{RF} is given in MV for R in km.

The quantity $\Delta(\beta\gamma)_{st}$ in Table II and Fig 8 is the full width of the distribution at half-height. Making the approximation that this is roughly equal to the half-width at the base of the distribution, $\Delta(\beta\gamma)_{st}$ may be used directly in equ (25a). The resulting voltages for the worst case, (k_{max} = 250 T/m), are listed in Table III.

TABLE III

RF VOLTAGE , k = 250T/m.

P (TeV/c)	20	40	60	80	100
R (km)	12.46	24.91	37.37	49.82	62.28
Q	208.25	292.25	356.25	412.25	460.25
$\Delta(\beta\gamma)_{st}$	4.00	6.73	9.12	11.32	13.38
V_{RF} (MV)	1.42	2.04	2.52	2.90	3.25

Even allowing for the approximations involved in this calculation, the voltage requirements seem to be very reasonable.

7. CONCLUSIONS

Based on existing lattice design techniques but using niobium-tin superconductor, these high energy coasting-beam p-p storage rings appear to present no insuperable technical difficulties. Luminosities of order 10^{32} $cm^{-2}s^{-1}$ per crossing seem possible, even though only single-turn filling has been contemplated: greater values could be achieved by stacking further turns, if the resulting currents and stored energies could be controlled.

Stored energy in the beams reaches very high levels by present-day standards - for instance 1.92 GJ per beam at 20 TeV. However, this beam has a revolution time of about 260 μs, so that dumping procedures which deal with sections of a few kilometres may be contemplated and could reduce the problem considerably.

We have studied designs in which the vacuum chamber bore is several centimetres radius, even though the beam itself should occupy only a fraction of a millimetre. This approach may be necessary from vacuum considerations, as well as from the point of view of practical magnet design. One outcome is that there should be space to spare for closed orbit correction; and that once the correction has been achieved, the beam should occupy an excellent 'good-field' region, with consequent relative freedom from non-linear effects. However, these features of the design have to be examined in greater detail to verify such arguments.

Siting and cost are problems which we have not considered seriously as yet. No doubt both are formidable, but do not seem to constitute technical limitations.

The provision of electrical power for the entire accelerator and storage ring complex presents a severe practical problem. One suggestion we offer for future consideration: namely, to power the complex with an accelerator-driven heavy ion fusion plant.

ACKNOWLEDGEMENTS

The authors wish to thank M Hanney and Y Marti of the CERN ISR Division for their assistance in using the programs AGS and STORPA2.

REFERENCE

(1) E Keil. Perspectives on Colliding Beams. Proc. 8th Inter. Conf. on High Energy Accels., Stanford, p660, (1974).

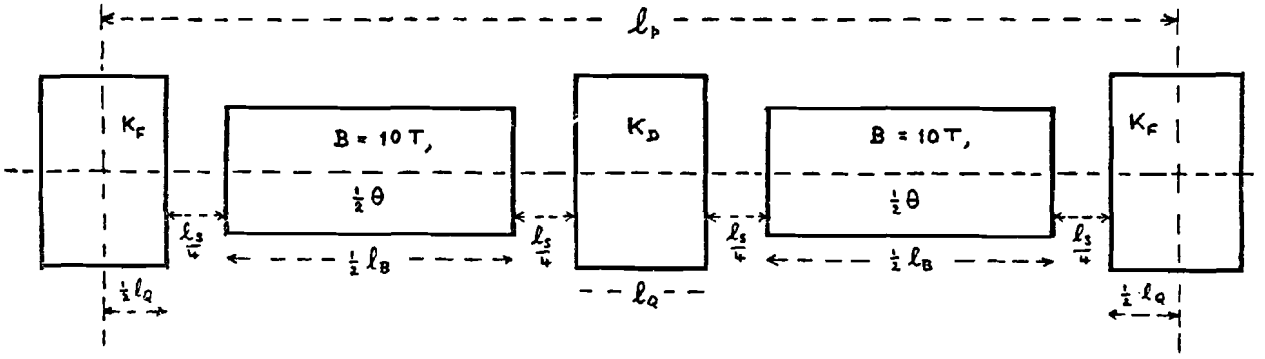

FIG. 1 SCHEMATIC NORMAL CELL

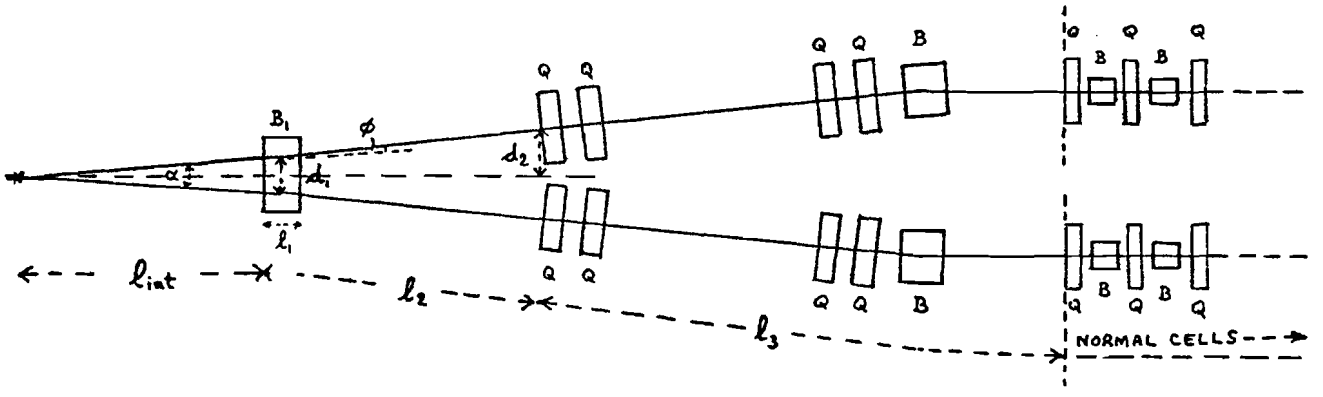

FIG. 2 SCHEMATIC HALF-INSERTION

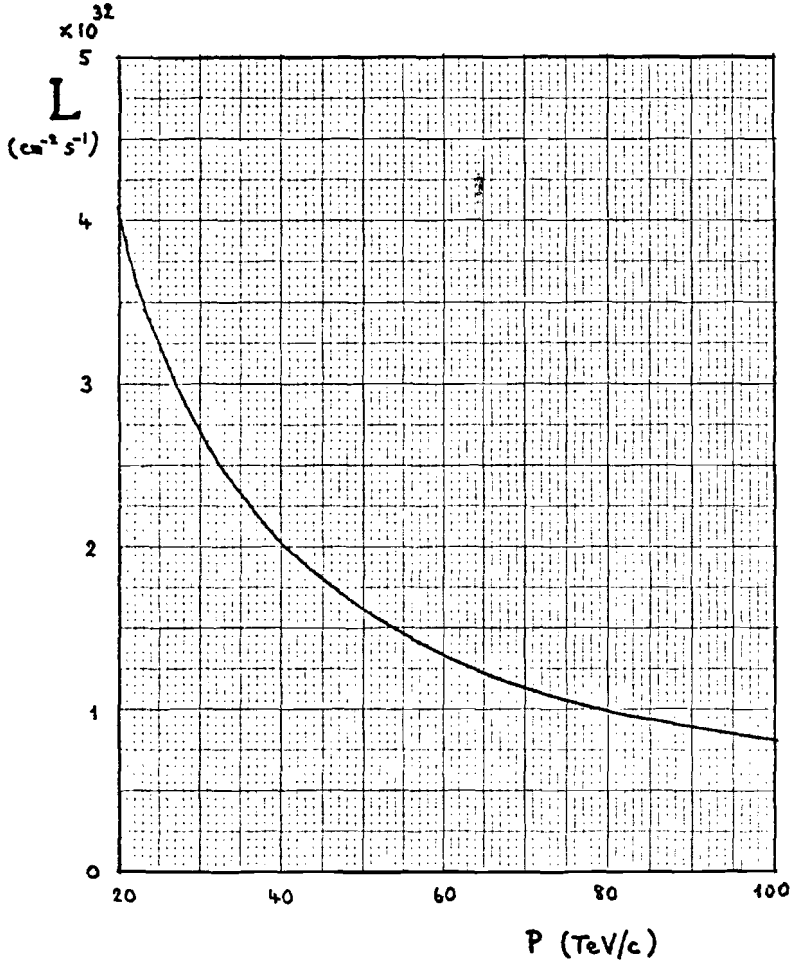

FIG. 3 LUMINOSITY

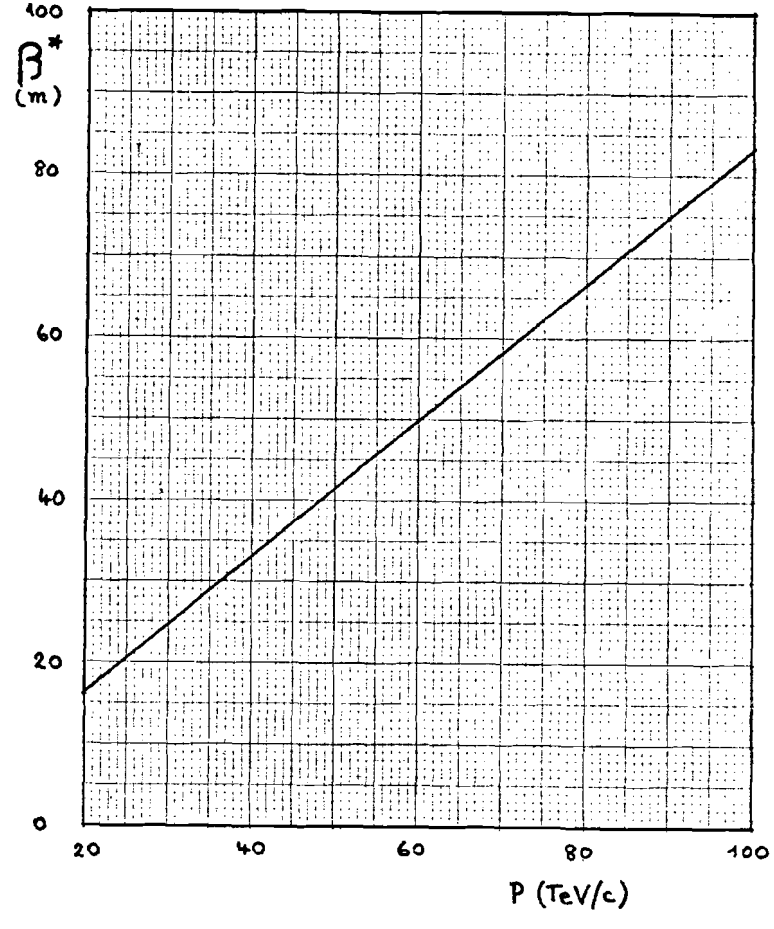

FIG. 4 β^*

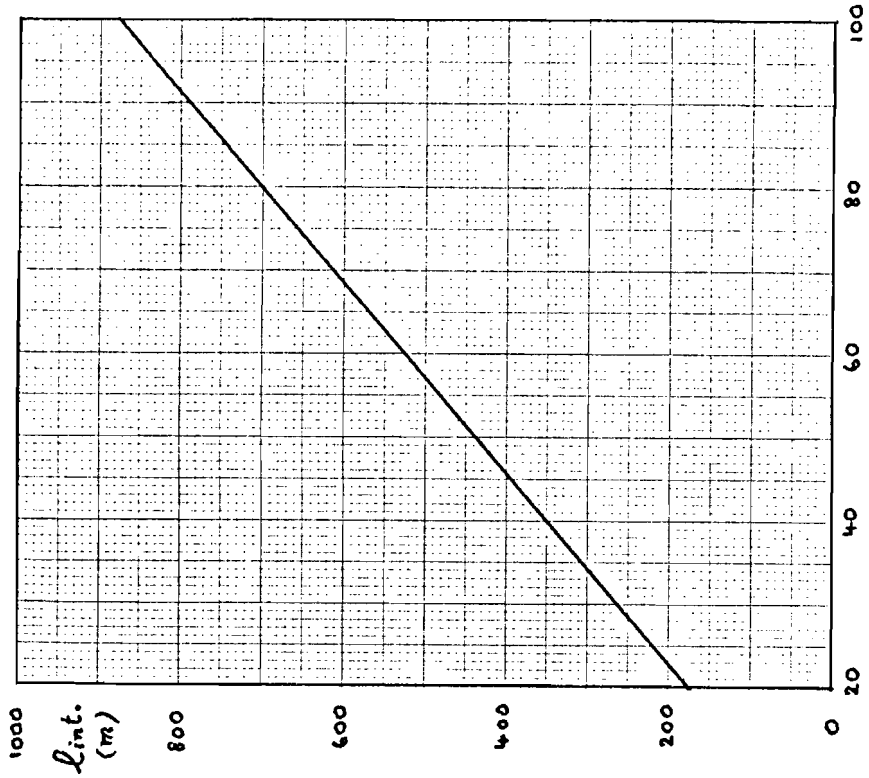

FIG.6 FREE SPACE ℓ_{int}

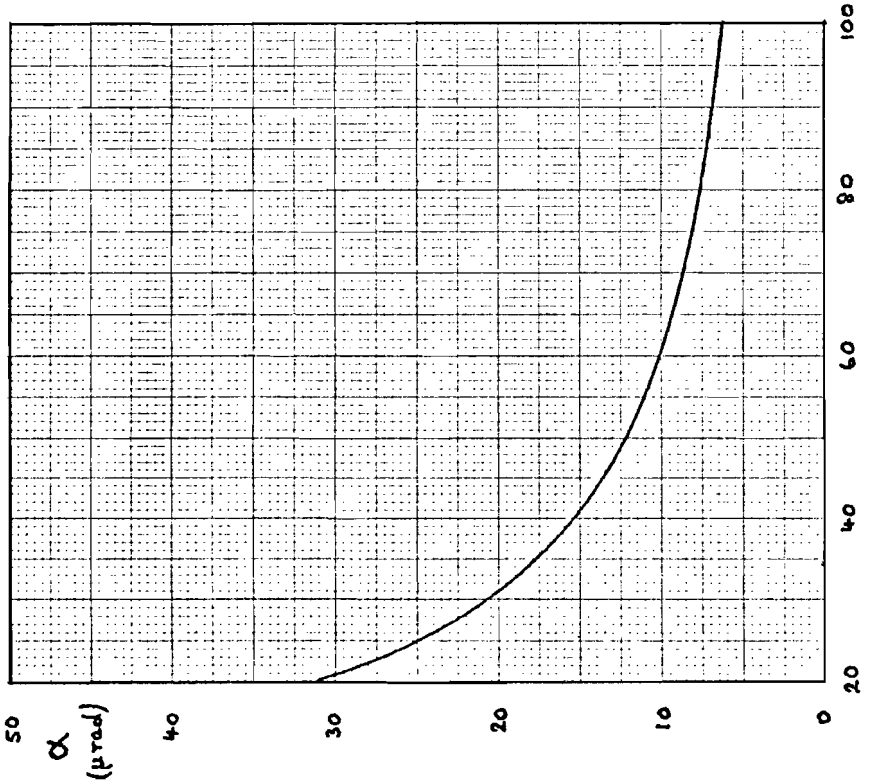

FIG.5 CROSSING ANGLE

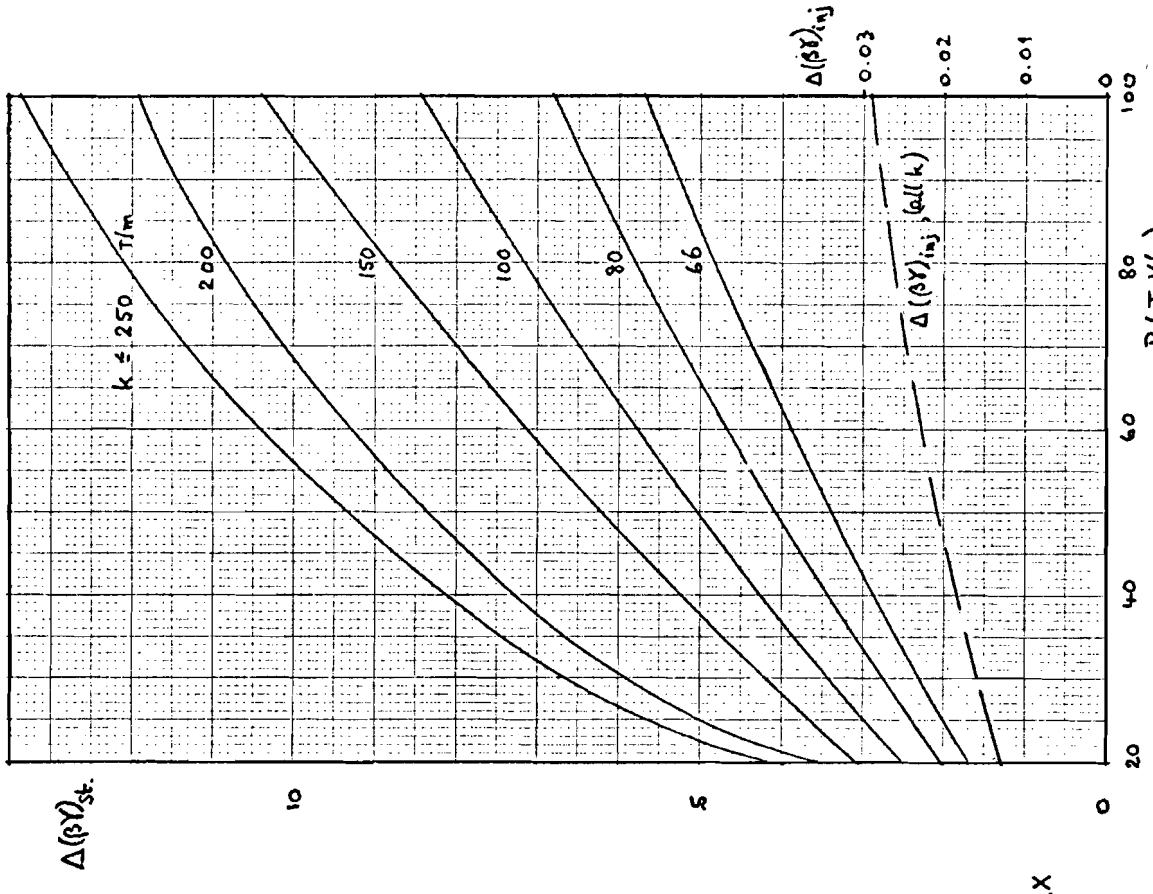

FIG. 8 $\Delta(\beta\gamma)$ SPREAD

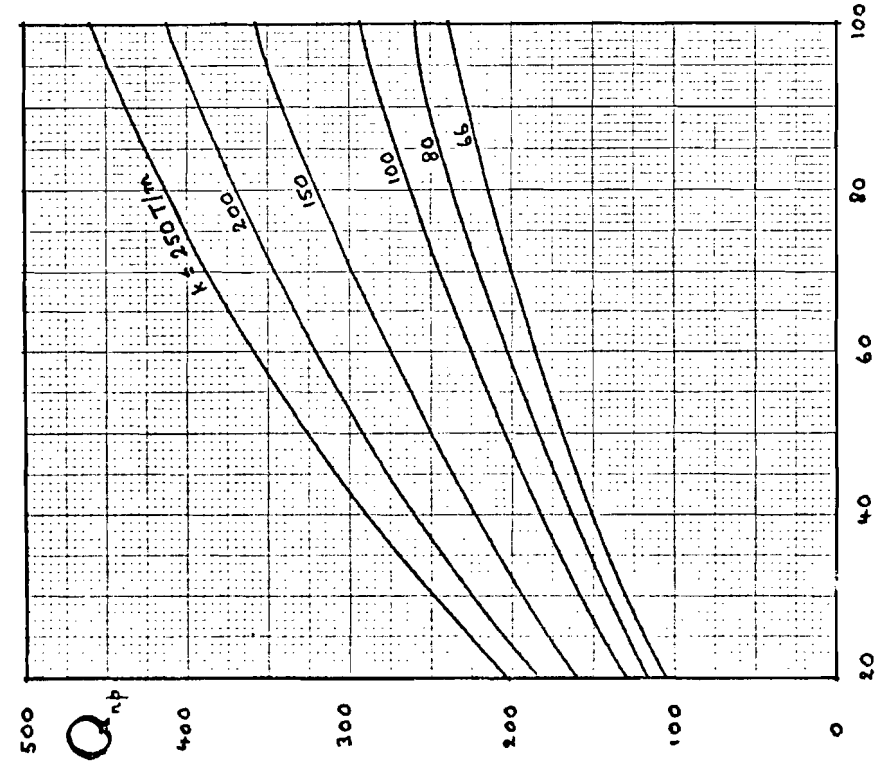

FIG. 7 VALUES DIFFERENT k_{max}